Hindawi
Advances in Polymer Technology
Volume 2019, Article ID 9679627, 10 pages
https://doi.org/10.1155/2019/9679627

Research Article

The Influence of Mg^{2+} Ions on the *In Vitro* Efficacy of Chitosan-Titanium Dioxide Nanotubes (CTNTs) Scaffolds

Siew Shee Lim,[1] **Shui Wei Kho**,[1] **Nehemiah Li Heng Ang**,[1] **Cheng Heng Pang**,[2] **and Hwei-San Loh**[3]

[1]*Department of Chemical and Environmental Engineering, University of Nottingham Malaysia Campus, Jalan Broga 43500 Semenyih, Selangor, Malaysia*
[2]*Department of Chemical and Environmental Engineering, University of Nottingham Ningbo China, 199, Taikang East Road, Ningbo 315100, China*
[3]*School of Biosciences, University of Nottingham Malaysia Campus, Jalan Broga 43500 Semenyih, Selangor, Malaysia*

Correspondence should be addressed to Siew Shee Lim; siewshee.lim@nottingham.edu.my and Hwei-San Loh; sandy.loh@nottingham.edu.my

Received 30 October 2018; Accepted 30 December 2018; Published 20 January 2019

Academic Editor: Lucia Baldino

Low mechanical strength and lack of osteoconductive cues are problems associated with chitosan-based scaffolds. This research aimed to fabricate reinforced chitosan-titanium dioxide (TiO_2) nanotubes (CTNTs) scaffolds attributed to the enhanced biocompatibility and physical properties of TiO_2 nanotubes (TNTs). The incorporation of hydrothermally synthesized TNTs at weight percent of 16 into chitosan was achieved via direct blending and lyophilization. CTNTs scaffolds were further subjected to 24-h adsorption in $MgCl_2$ solutions of 0.5 mM, 1 mM, 2.5 mM, and 5 mM at physiological pH. The adsorption affinity of CTNTs towards Mg^{2+} ions was high and mainly attributed to the macroporosity of scaffolds and nanocavities of TNTs. The maximum monolayer adsorption capacity of CTNTs for Mg^{2+} ions was 8.8 mg/g scaffolds. Its adsorption isotherm fitted well with Langmuir isotherm by showing R^2 of 0.9995. Fluorescence-based staining, cell viability, and alkaline phosphatase assays indicated that the adsorbed Mg^{2+} ions onto CTNTs scaffolds aided in promoting higher proliferation and early differentiation of MG63 cells than scaffolds without Mg^{2+} ions in a concentration-dependent manner. Based on current results, CTNTs scaffolds with Mg^{2+} ions may be a potential biomaterial for bone regeneration.

1. Introduction

Degenerative bone diseases such as osteoporosis and osteoarthritis, accidental bone fractures, resection of primary tumors, and traumatic skeletal injuries that dramatically affect patients' functional status have a significant impact on the world population particularly the elderly. Scaffold-aided surgical intervention is therefore required to facilitate the limited ability of bone tissues to repair and regenerate [1].

Bone scaffolds serve as a temporary support at bone defective sites, which guide the bone formation in a controlled manner and then degrade after the new bone formation. Types of materials determine the physiochemical properties of scaffolds such as mechanical strength, pore size, and porosity. Synthetic or natural polymers have been extensively studied for bone regeneration. They are fabricated as scaffolds with high porosity and pore size which allow matching their degradation rate with that of bone formation. The additional functions of scaffolds are to promote cellular infiltration and vascularization [2]. Chitosan has been reported as a preferable material more than other synthetic ones due to its high hydrophilicity [3], moldability [4], biodegradability [5], and nontoxicity [6]. Yet pure chitosan scaffolds lack mechanical strength and are also less osteoconductive [7].

Advantageous interactions between nanobiomaterials and osteoblasts (bone-forming cells) were observed in many studies [8–13]. This was attributed to the strong resemblance of nanomaterials to bone entities such as fibril collagen and nanocrystal hydroxyapatite [14]. Particularly, the hydrothermally synthesized titanium dioxide (TiO_2)

nanotubes (TNTs) inserted into rat femurs had shown a good evidence on new bone formation starting on day 7 [13]. Besides, a more recent *in vitro* study also showed that chitosan-TNTs scaffolds promoted the osteoblastic functions, i.e., adhesion, proliferation, and early differentiation [12].

The osteoconductive property of scaffolds can be greatly improved via the immobilization of cell adhesive proteins such as fibronectin, vitronectin, and tripeptide like Arg-Gly-Asp (RGD). The manipulation of these proteins and peptide on bone scaffolds with cell adhesive promoting conformation has remained a great challenge. This is attributed to the unpredictable conformational change in these biocues upon their adsorption on the surface of bone scaffolds as well as the questionable availability of RGD epitope in these proteins [15]. In addition, the incorporation of these cell adhesive proteins to the scaffolds has unlikely increased the overall cost of treatment.

A study on the effect of magnesium (Mg^{2+}) ions on alumina was performed and indicated that substrata with Mg^{2+} ions promoted better osteoblast adhesion via an integrin-mediated mechanism [16]. Besides that, higher osteoblastic adhesion was also observed on apatite with Mg^{2+} ions by Yamasaki et al. [17] and composite containing Mg^{2+} ions by Okazaki et al. [18]. All these works suggested that the immobilization of Mg^{2+} ions on chitosan scaffolds which lack osteoconductive cues would increase their biocompatibility. More importantly, the success of immobilization or functionalization of Mg^{2+} ions onto the chitosan scaffolds may replace the use of abovementioned costly cell adhesive proteins which possesses an economic importance for patients suffering bone diseases.

This paper describes the novel chitosan composite scaffolds incorporated with hydrothermally synthesized TNTs (CTNTs) and functionalized with different concentrations of Mg precursor solution through liquid-solid adsorption at physiological pH whose combination has not been reported previously. The concentrations of Mg precursor solution used were 0.5 mM, 1 mM, 2.5 mM, 5 mM, 7.5 mM, and 10 mM which fell within the biocompatible range. The adsorption affinity of CTNTs was determined and fitted with Langmuir, Freundlich, and Temkin models. Three preliminary *in vitro* assays were then carried out on human osteosarcoma (MG63) cell line to investigate the biocompatibility and osteoblastic functions of the newly developed CTNTs scaffolds upon the effects of adsorbed Mg^{2+} ions.

2. Experimental

2.1. Materials. Titanium dioxide (TiO_2) powder, sodium hydroxide (NaOH) pellets, chitosan powder (middle viscous, 80% deacetylation), magnesium chloride hexahydrate ($MgCl_2.6H_2O$), fluorescein diacetate (FDA), sodium pyruvate, dimethyl sulfoxide (DMSO), and p-nitrophenyl phosphate (pNPP) were purchased from Sigma Aldrich, Germany. HCl (37% fuming) was purchased from Merck, Germany, while acetic acid and absolute alcohol (denatured) were purchased from R&M Chemicals, UK. Minimum essential medium (MEM) powder, fetal bovine serum (FBS), penicillin/streptomycin (Pen-Strep), and 3-(4, 5 dimethylthiazol-2-yl)-2, 5-diphenyltetrazolium bromide (MTT) were purchased from Gibco Laboratories, USA. PRO-PREP™ protein extraction solution was purchased from iNtRON Biotechnology, South Korea. Salts used to prepare phosphate-buffered saline (PBS) including sodium chloride (NaCl), potassium chloride (KCl), disodium phosphate (Na_2HPO_4), and monopotassium phosphate (KH_2PO_4) were purchased from R&M Chemicals, UK. All chemicals were used as received and all working solutions were prepared in distilled water.

2.2. Hydrothermal Synthesis and Characterization of TiO_2 Nanotubes (TNTs). The synthesis of TNTs was duly performed by the following method of Chen et al. [19] and Morgado et al. [20]. Prior to 72-h hydrothermal synthesis at 130°C, 2 g of TiO_2 was mixed with 40 mL of NaOH for 10 min and transferred to a Teflon lined stainless steel autoclave. The molarity of NaOH used was 10 M. The hydrothermally synthesized powder was then washed with 200 mL of 0.1M HCl and deionized water until the filtrate pH of 7 was achieved. The neutral powder was further calcined to 400°C for 5 h.

The surface morphology of the resultant powder was characterized by using Field Emission Scanning Electron Microscope (FESEM, Quanta 400, USA) at an accelerating voltage of 15 kV. The crystallinity of the hydrothermally synthesized TNTs powder was examined by using X-ray Powder Diffraction (XRD, Hiltonbrooks DG3 generator coupled with Philips PW1050/25 goniometer) with CuKα radiation at 50 kV/30 mA and a scanning speed of 1°/min.

2.3. Fabrication and Functionalization of Chitosan-TiO_2 Nanotubes (CTNTs) Scaffolds with Mg^{2+} Ions. Chitosan solution (1% v/v) was prepared by stirring 1 g of chitosan powder in 100 mL of 0.2 M acetic acid for 3 h. Chitosan solution was then mixed with 16 weight percent (wt%) of TNTs for 5 h. After homogeneous mixing, each well of 24-well plate was instantly filled with 1 mL of chitosan-TNTs (CTNTs) mixture. This plate was firstly subjected to 24-h freezing at -20°C and followed by freeze-drying at -40°C for 24 h. The rehydration of freeze-dried CTNTs scaffolds was performed by immersing them in 100%, 70%, and 50% of ethanol for 1 h, 30 min, and 30 min, respectively. Scaffolds were then dried in a desiccator.

The functionalization of CTNTs scaffolds with $MgCl_2$ was carried via liquid-solid adsorption. CTNTs scaffolds were firstly immersed in 100-mL Schott bottles filled with 20 mL of $MgCl_2$ solution (0.5 mM, 1 mM, 2.5 mM, 5 mM, 7.5 mM, and 10 mM corresponding to 12.15 mg/L, 24.3 mg/L, 60.76 mg/L, 121.53 mg/L, 182.28 mg/L, and 243.05 mg/L of Mg as $CaCO_3$, respectively). The Schott bottles were closed and placed in an orbital shaker (Unimax 1010, Germany) and shaken at 100 rpm for 24 h. The Schott bottles were taken after 24 h and the final concentration of Mg^{2+} ions was analyzed by using a preprogrammed spectrophotometer (HACH, USA) and Ca/Mg hardness kit (HACH, USA). Each experiment was conducted in triplicate under identical operating conditions. The amount of adsorbed Mg^{2+} ions onto CTNTs scaffolds

was then determined by using (1). The Mg^{2+}-functionalized scaffolds were washed with deionized water and dried prior conducting the *in vitro* tests.

$$q_e = \frac{(C_o - C_e)V}{M} \quad (1)$$

where q_e is the amount of Mg^{2+} ions adsorbed by per gram scaffold (mg/g), C_o and C_e are the concentrations of $MgCl_2$ solutions before and after functionalization (mg/L), respectively, V is the volume of $MgCl_2$ solution (L), and M is the mass of dried CTNTs scaffold (g).

The adsorption of Mg^{2+} ions onto CTNTs scaffolds was also analyzed by using Langmuir, Freundlich, and Temkin isotherm models. Langmuir isotherm assumes monolayer adsorption on homogenous surface with a finite number of adsorption sites. The mathematical representation of Langmuir isotherm is shown in

$$\frac{C_e}{q_e} = \frac{1}{bq_m} + \frac{C_e}{q_m} \quad (2)$$

where q_m is the maximum adsorption capacity per unit weight of scaffold for Mg^{2+} ions (mg/g) and b is the Langmuir isotherm constant (L/mg).

Freundlich isotherm is generally applied to express multilayer adsorption on heterogeneous surface of adsorbents. The Freundlich isotherm is represented in

$$\ln q_e = \ln K_F + \frac{1}{n} \ln C_e \quad (3)$$

where K_F is the adsorption capacity of scaffolds $[mg/g(L/mg)^{1/n}]$ and $1/n$ represents the adsorption intensity or surface heterogeneity [21].

Temkin isotherm model assumes the interactions between Mg^{2+} ions. The heat of adsorption of all molecules in the layer would decrease linearly with the coverage caused by adsorbate/adsorbate interactions [22]. The mathematical representation of Temkin model is shown in

$$q_e = B \ln K_t + B \ln C_e \quad (4)$$

where K_t is an equilibrium binding constant (L/mg) corresponding to the maximum binding energy and B is related to the heat of adsorption.

2.4. In Vitro Cell Culture. The biocompatibility of CTNTs scaffolds with and without Mg^{2+} ions was evaluated by using human osteosarcoma (MG63) cell line (ATCC, USA). MG63 cells were maintained using MEM supplemented with 10% (v/v) FBS, 1% (v/v) Pen-Strep, and 1% (v/v) 1 mM sodium pyruvate at 37°C in a humidified 5% CO_2 atmosphere. For subculture, cells were detached by 0.25% trypsin and plated in 75-mL flask every 3-4 days. For all *in vitro* assays, cells were detached via trypsinization after the cell confluence of 90-100% was achieved. Prior to cell seeding, cell count was performed using Haemacytometer (Hirschmann Laborgerate, Germany). CTNTs scaffolds with different amounts of adsorbed Mg^{2+} ions (treatment group) and scaffolds without Mg^{2+} ions (negative control group) were placed into 24-well plates and sterilized with UV radiation for 15 min. Each scaffold and polystyrene surface of 24-well plates was seeded with 3 x 10^4 of MG63 cells. Cells grown on polystyrene well without scaffolds were served as a positive control. The cells were then incubated at 37°C for predetermined incubation periods as specified in the respective assays. The media were changed every 3 days.

2.5. Vital Fluorescein Diacetate (FDA) Staining Assay. Vital staining was performed with 3 μg/mL of FDA in PBS. The conversion of FDA to fluorescein form by esterase of living cells is used to determine the cellular survival histologically. The treatment (scaffolds with Mg^{2+}), negative control (scaffolds without Mg^{2+}), and positive control (polystyrene well) groups were seeded with 3 x 10^4 of MG63 cells and incubated for 3, 5, and 7 days. After each incubation period, cells grown on CTNTs scaffolds and polystyrene well were washed in PBS and stained with 3 μg/mL of FDA in PBS for 5 min. Staining solution was then removed and following a washing step with PBS, the samples were viewed under a fluorescence microscope (Nikon AZ100, Japan). FDA images were analyzed via ImageJ™ software. The percentages of FDA-stained cells based on three independent experiments were calculated by the ratio of the number of pixels showing FDA stain to the total number of pixels in the image.

2.6. 3-(4, 5 Dimethylthiazol-2-yl)-2, 5-Diphenyltetrazolium Bromide (MTT) Assay. The proliferation rates of MG63 cells on the treatment (scaffolds with Mg^{2+}), negative control (scaffolds without Mg^{2+}), and positive control (polystyrene well) groups were evaluated by using MTT (Invitrogen, USA) which is a common cell viability assay [23]. Similar to FDA staining assay, 3 x 10^4 of MG63 cells were seeded on the treatment, negative control, and positive control groups and incubated for 3, 5, and 7 days. After each incubation period, 100 μL of MTT solution was added to each well and left for 4 h. The initial color of MTT solution was reduced to purple crystals, when MG63 cells had responded to the MTT solution. This was followed by the addition of 1 mL of DMSO to dissolve the purple crystals. Absorbance on the wells indicating the extent of osteoblastic proliferation was measured as optical density (OD) values in six times by using Varioskan™ Flash Multimode Reader (Thermo Scientific, USA) at the wavelength of 570 nm.

2.7. Alkaline Phosphatase (ALP) Assay. The early differentiation marker, ALP, was used to evaluate the osteoblastic differentiation of MG63 cells on CTNTs scaffolds with and without Mg^{2+} ions in comparison to the positive control cells grown on polystyrene well. Complete growth medium was supplemented with 50 μg/mL ascorbic acid and 10 mM β-glycerophosphate. Similarly, the treatment (scaffolds with Mg^{2+}), negative control (scaffolds without Mg^{2+}), and positive control (polystyrene well) groups were seeded with 3 x 10^4 of MG63 cells and incubated for 7, 14, and 21 days. Then, the culture medium was removed from each well and then

washed with PBS twice. Subsequently, CTNTs scaffolds with cells (treatment and negative control groups) and cells grown on polystyrene well (positive control group) were scraped and incubated with 500 μL of PRO-PREP solution on ice to obtain the protein lysates. The cellular ALP activity was calculated as the rate of p-nitrophenyl phosphate (pNPP) being hydrolyzed by ALP into p-nitrophenol. In a 96-well plate, 100 μL of pNPP was added to 100 μL of cell lysates and incubated for 2 h at 37°C. The absorbance (OD) was then measured at 405 nm by using Varioskan™ Flash Multimode Reader (Thermo Scientific, USA) to detect the p-nitrophenol level. Six independent experiments were conducted for each incubation period.

2.8. Statistical Analysis. All quantitative data were presented as the mean ± standard error of the mean values from at least three independent experiments. The collected quantitative data of *in vitro* assays were analyzed and compared by using Student's t-test or ANOVA with Bonferroni as a post hoc test depending on the data distribution as suggested [24]. A p value of less than 0.05 was considered to be statistically significant.

3. Results and Discussion

3.1. Characterization of TNTs. The crystallinity and dimension of TNTs were reported to influence their biocompatibility. Among crystal phases, anatase is the most biocompatible phase. TNTs with diameter ranging between 20-70 nm promoted better osteoblastic proliferation and differentiation [25]. Therefore, the characterization of TNTs was carried out before the direct blending with chitosan solution to ensure their biocompatible crystal phase and homogeneity in the composite scaffolds. The surface morphology of TNTs was examined by using FESEM and is shown in Figure 1. These loose bundles of TNTs exhibited high degree of agglomeration and aggregation due to their high surface energy. The length of TNTs was observed ranging from a few hundred nanometres to one micrometre. Notably, the diameter of TNTs fell within the optimum range which persuasively pushed forward the evaluation of their *in vitro* biocompatibility.

The XRD analysis showed changes in crystal phase before and after heating at 400°C. No distinct TiO_2 diffraction peaks were observed in Figure 2 spectrum (a) which suggests that 72-h synthesis and the subsequent washing step completely converted the starting materials to amorphous particles. However, the crystallinity of heated TNTs became distinguished. All diffraction peaks of 25.4°, 37.8°, 48.0°, and 54.5° in Figure 2 spectrum (b) corresponded to the crystal phase of anatase. The heating at 400°C resulted in slow dehydration and dehydroxylation of TNTs. This was instantly accompanied by a decrease in interlayer spacing of the nanotube walls which in turn increased their crystallinity [26]. The heated TNTs were in anatase phase which matched the formation principle of hydroxyapatite on TiO_2 surface [27]. The XRD pattern of heated TNTs again confirmed that heating at 400°C is necessary for the anatase conversion.

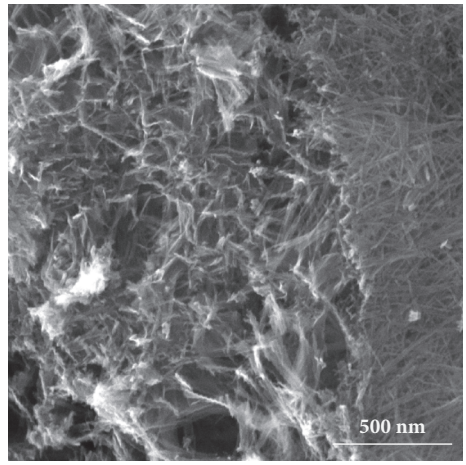

Figure 1: FESEM image of TNTs prepared via 72-h hydrothermal synthesis at 130°C and after heating at 400°C for 5 h.

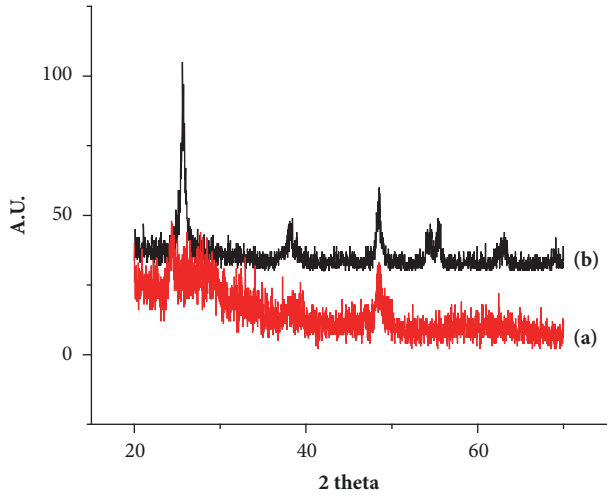

Figure 2: XRD spectra of hydrothermally synthesized powder (a) before and (b) after heating at 400°C.

Again, this crystal phase would play a key role in the immobilization of Mg^{2+} ions onto the scaffolds.

3.2. Functionalization of CTNTs Scaffolds with Mg^{2+} Ions. CTNTs scaffolds were functionalized with different concentrations of $MgCl_2$ via liquid-solid adsorption at pH 7.2. The amount of Mg^{2+} ions adsorbed onto CTNTs scaffolds (q_e) and the concentration of $MgCl_2$ solution after functionalization (C_e) were measured and recorded in Figure 3. The amount of Mg^{2+} ions adsorbed by CTNTs scaffolds increased from 1.45 mg/g to 8.8 mg/g corresponding to the initial concentration (C_o) of $MgCl_2$ solution from 12.15 mg/L (0.5 mM $MgCl_2$) to 243.05 mg/L (10 mM $MgCl_2$), respectively. The adsorption isotherm of Mg^{2+} ions onto CTNTs scaffolds was indicative of a favorable adsorption trend. There was a rapid increase in the uptake of Mg^{2+} ions at C_e value of 12 mg/L, as the resistance to the mass transfer of Mg^{2+} ions between aqueous and solid phases was overcome by the gradual increase of

$MgCl_2$ concentration. Eventually, this adsorption isotherm ended with a plateau at the C_e range from 50 to 180 mg/L. This indicates the saturation of CTNTs scaffolds with Mg^{2+} ions in a monolayer manner and the highest amount of adsorbed Mg^{2+} ions was 8.8 mg/g. The CTNTs scaffolds showed a high affinity towards Mg^{2+} ions thus readily promoting the monolayer formation of adsorbed Mg^{2+} ions. As the q_e values for scaffolds functionalized with $MgCl_2$ at the initial concentrations of 121.53 mg/L and 243.05 mg/L solution were closely to 8.8 mg/g, the *in vitro* tests were conducted on CTNTs scaffolds functionalized at the initial concentrations between 12.15 mg/L (0.5 mM $MgCl_2$) and 121.53 mg/L (5 mM $MgCl_2$). These effects of different amounts of Mg^{2+} ions adsorbed onto CTNTs scaffolds in influencing the osteoblastic response were then evaluated.

Besides, the adsorption isotherm of Mg^{2+} ions onto CTNTs scaffolds was also analyzed by using Langmuir, Freundlich, and Temkin models. The correlation coefficient (R^2) derived from each model was compared to determine the applicability of isotherm models and the nature of adsorption. Graphs representing Langmuir, Freundlich, and Temkin isotherms were plotted and shown in Figures 4(a), 4(b), and 4(c), respectively. The respective slope and intercept for each graph were calculated and tabulated in Table 1. Based on the fitting of three isotherms, Langmuir isotherm model best fitted with the experimental data by showing the highest R^2 value of 0.9995 as compared to the other two models. This finding was also in a good agreement with the plateau observed in Figure 3. It is confirmed that the monolayer coverage of Mg^{2+} ions onto CTNTs scaffolds and its adsorption involved were chemisorption. As a result, desorption of Mg^{2+} ions from the surface of scaffolds is not likely. These immobilized Mg^{2+} ions are expected to have direct interactions with bone scaffolds leading to subsequent osteoblastic functions which include proliferation and differentiation.

3.3. Cell Vitality Observation. The ability of scaffolds in promoting proliferation is very crucial to bone regeneration, as enhanced cellular proliferation ultimately leads to new bone tissues formation. In order to determine the effects of Mg^{2+} ions on the proliferation of MG63 cells histologically, living cells cultured on the CTNTs scaffolds with and without Mg^{2+} ions for 3, 5, and 7 days were stained with FDA and subjected to fluorescence microscopic observation. These FDA-stained cells on scaffolds were compared to cells directly cultured on polystyrene well (positive control). The percentages of FDA-stained cells on scaffolds and polystyrene well are presented in Figure 5. Representative images of FDA-stained MG63 cells cultured on CTNTs scaffolds with and without Mg^{2+} ions at different time intervals are shown in Figure 6.

MG63 cells did not spread nicely on scaffolds without Mg^{2+} ions [Figures 6(a) and 6(g)] and scaffolds functionalized with 0.5 mM $MgCl_2$ even after 5-day culture [Figures 6(b) and 6(h)]. Direct interaction between MG63 cells and CTNTs scaffolds without Mg^{2+} ions was found to be an inhibitory effect even when the crystal phase of TNTs was converted to anatase. This could be due to the slightly acidic

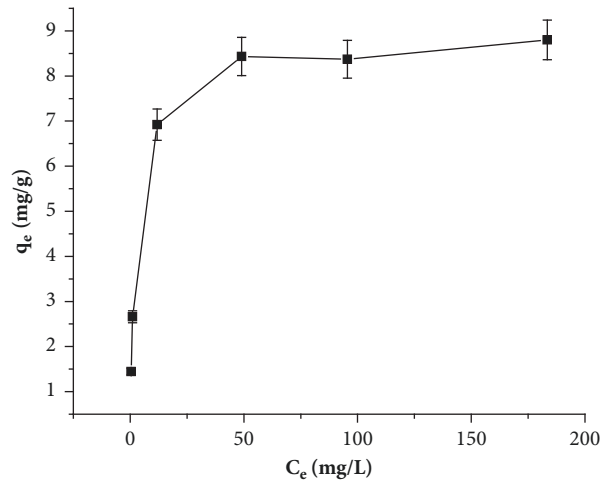

Figure 3: Adsorption isotherm of Mg^{2+} ions onto CTNTs scaffolds as measured at pH 7.2 after 24 h.

Table 1: Isotherm parameters for adsorption of Mg^{2+} ions onto CTNTs scaffolds.

Isotherms	Constants	R^2
Langmuir	q_m (mg/g) = 8.88 b (L/mg) = 0.3283	0.9995
Freundlich	1/n = 3.396 K_F = 2.3715	0.8830
Temkin	K_t = 8.913 B = 1.2847	0.9514

nature of chitosan-based scaffolds. The low survival of MG63 cells on CTNTs scaffolds functionalized with 0.5 mM $MgCl_2$ after 5 days of culture suggests that the amount of adsorbed Mg^{2+} ions was not sufficient to promote a rapid osteoblastic proliferation. However, the percentage of FDA-stained cells cultured on CTNTs scaffolds functionalized with 0.5 mM $MgCl_2$ was increased on 7-day culture, i.e., 2 days later.

Unlike on scaffolds without Mg^{2+} ions, MG63 cells were found scattered on CTNTs scaffolds functionalized with 1 mM, 2.5 mM, and 5 mM $MgCl_2$ as shown in Figure 6. Their proliferation on these materials took place in a progressive manner by showing a gradual increase in the percentage of FDA-stained cells over time (Figure 6). Overall, the highest abundance of FDA-stained cells was observed in cells cultured on polystyrene well (positive control) after 5 and 7 days of incubation ($p<0.001$). Cells also showed a higher vitality on CTNTs scaffolds functionalized with 1 mM, 2.5 mM, and 5 mM $MgCl_2$ on 5 and 7 days. This indicates that high adaptation of MG63 cells on the scaffolds functionalized with $MgCl_2$ at the concentration more than 1 mM has occurred and this higher concentration is necessary to overcome the inhibitory effect of sole scaffolds by increasing their pH to reach the physiological state. This also verified that no desorption of Mg^{2+} ions has occurred under this physiological condition.

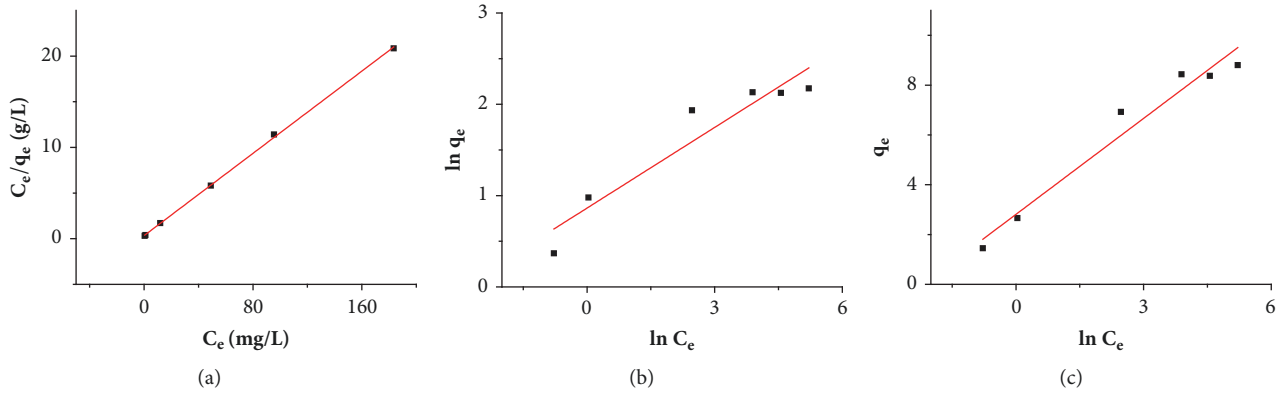

Figure 4: (a) Langmuir, (b) Freundlich, and (c) Temkin isotherms for the adsorption of Mg^{2+} ions onto CTNTs scaffolds as measured at pH 7.2.

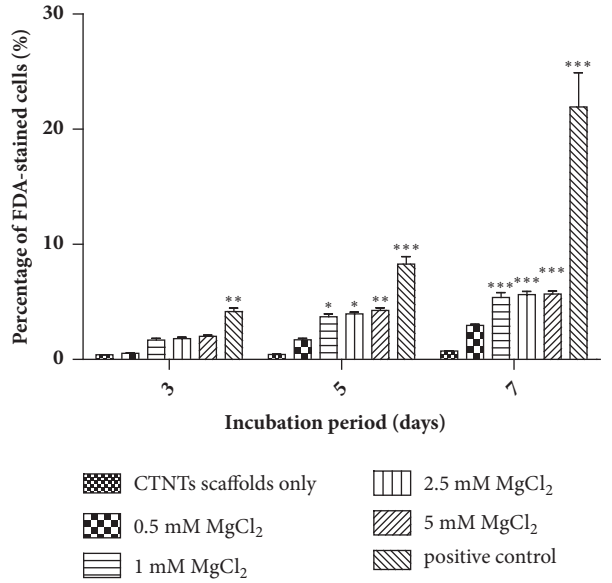

Figure 5: Percentages of FDA-stained cells cultured on polystyrene well (positive control), CTNTs scaffolds only and CTNTs scaffolds with different amounts of Mg^{2+} ions adsorbed at different initial concentrations (0.5-5 mM) of $MgCl_2$ for 3, 5, and 7 days (∗p<0.05, ∗∗p<0.01, ∗ ∗ ∗p<0.001, n = 3).

Meanwhile, there is a challenge seen in the quantification of FDA-stained cells on scaffolds, as some cells infiltrated into CTNTs scaffolds with Mg^{2+} ions instead of attaching on the surface of three-dimensional construct. This observation is in accordance with the similar chitosan composite scaffolds as constructed by Goh et al. [1] and Lim et al. [12], as MG63 cells possess a tendency of infiltration which could prepare them to enter into the following stage, i.e., early differentiation. Notably, immobilization of Mg^{2+} ions onto porous CTNTs scaffolds through liquid-solid adsorption also aids to provide a higher surface area for bone regeneration as compared to any two-dimensional constructs.

3.4. Cellular Proliferation Effect. Following the viable cells adhered on the scaffolds, proliferation of cells is expected. Figure 7 shows the proliferation effect of MG63 cells cultured on polystyrene well (positive control), CTNTs scaffolds without Mg^{2+} ions, and CTNTs scaffolds functionalized with different concentrations of $MgCl_2$ on the culture periods of 3, 5, and 7 days as evaluated by using MTT assay.

Consistently, CTNTs scaffolds without Mg^{2+} ions showed the lowest proliferation level regardless of incubation period where MG63 cells did not significantly grow even after 7 days as shown in Figure 7. This finding confirmed the inhibitory nature of CTNTs scaffolds and corroborated well with the histological results in the previous section. Such low biocompatible feature of CTNTs scaffolds was similar to pure chitosan membrane prepared by Amaral et al. [28] showing poor cellular proliferation after 7 days of culture too. Clearly, CTNTs scaffolds without Mg^{2+} ions lack of osteoconductive cues to facilitate osteoblastic growth. More importantly, the roughness of CTNTs scaffolds was encountered to be a great

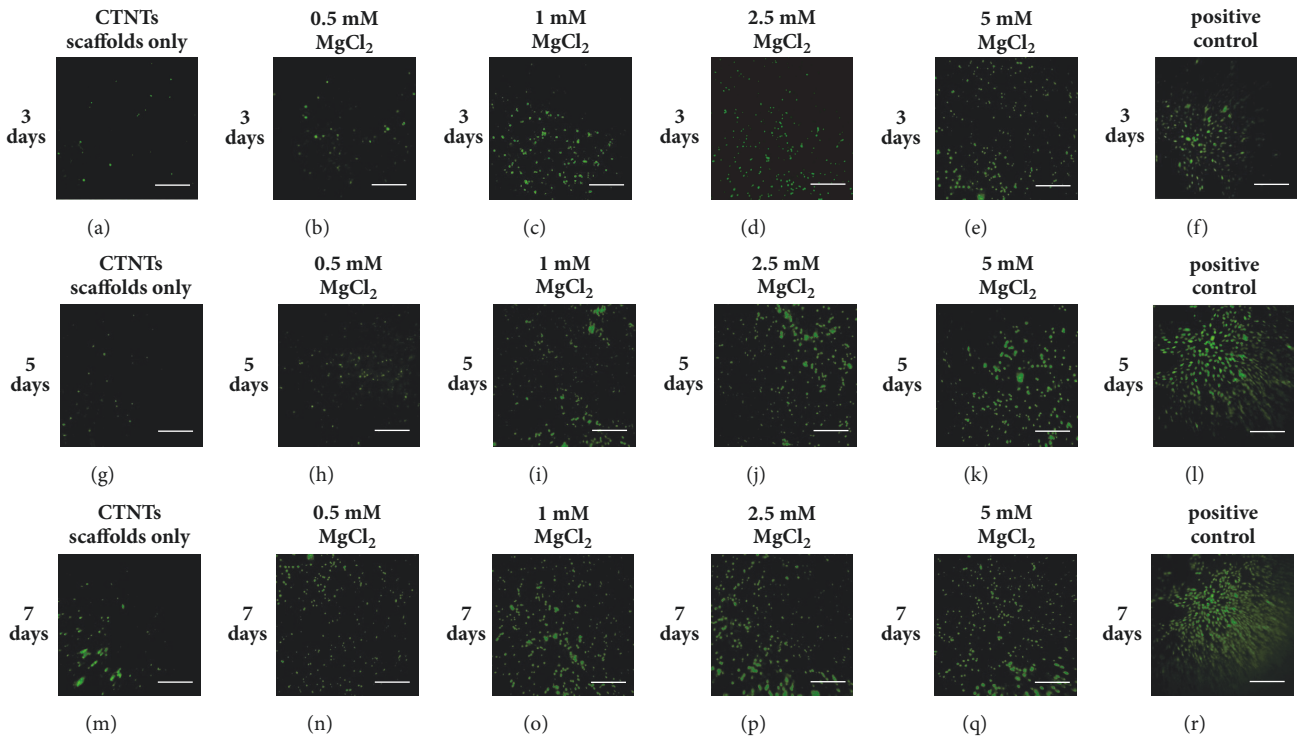

FIGURE 6: FDA-stained MG63 cells cultured on CTNTs scaffolds only and with Mg^{2+} ions adsorbed at different initial concentrations of $MgCl_2$ for 3 (a-f), 5 (g-l), and 7 (m-r) days. Scaffolds and polystyrene well (positive control) were seeded with approximately 30,000 cells/well in 24-well plates. Scale bar corresponds to 100 μm.

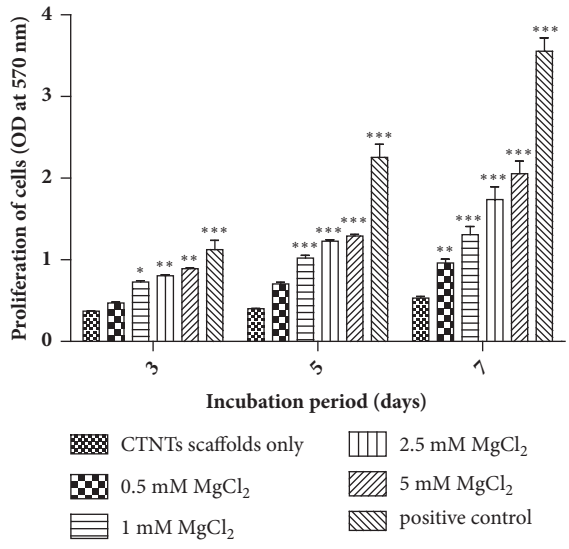

FIGURE 7: Proliferation effect of MG63 cells grown on CTNTs scaffolds only, CTNTs scaffolds functionalized with different concentrations of $MgCl_2$ and polystyrene well (positive control) as evaluated by MTT assay on the culture periods of 3, 5, and 7 days (∗ $p<0.05$, ∗∗ $p<0.01$, ∗ ∗ ∗$p<0.001$, n = 6).

challenge in accommodating focal contact formation for MG63 cells. MG63 as osteoblast-like cells can discriminate between surfaces with comparable roughness. The growth and phenotypic maturation of MG63 cells were performed better on smoother TiO_2-coated surfaces than on rougher uncoated substrates [29]. This hence clarified the impaired proliferation of MG63 cells on CTNTs scaffolds without Mg^{2+} ions which exhibited a certain degree of roughness.

The degree of proliferation of MG63 cells on CTNTs scaffolds with and without Mg^{2+} ions was different in spite of similarity in the microstructure of both types of scaffolds. Higher proliferation of MG63 cells on CTNTs scaffolds with Mg^{2+} ions was detected during 3-7 days ($p<0.001$). The proliferation of MG63 cells augmented with increasing amount of Mg^{2+} ions at each incubation period has demonstrated that cells responded to the amount of Mg^{2+} ions in a concentration-dependent manner. Among all CTNTs scaffolds with Mg^{2+} ions, the highest proliferation of MG63 cells was observed in scaffolds functionalized with 5 mM $MgCl_2$. Noticeably, extracellular Mg^{2+} ions on CTNTs scaffolds overcame the inhibitory effect of the scaffolds by elevating their proliferation level. It is suggested that the adsorbed Mg^{2+} ions act as osteoconductive cues which triggered the adhesion of MG63 cells on scaffolds via integrin-mediated mechanism [16, 30]. Integrin is an adhesion protein in cells responsible for mediating the cellular adhesion on biomaterials and its function is regulated by divalent cations like Mg^{2+} ions [30]. Adsorbed Mg^{2+} ions facilitate the interactions between scaffolds and MG63 cells which in turn promote the ability of cells to proliferate better. Of course, the proliferation of MG63 cells was still the highest on polystyrene well (positive

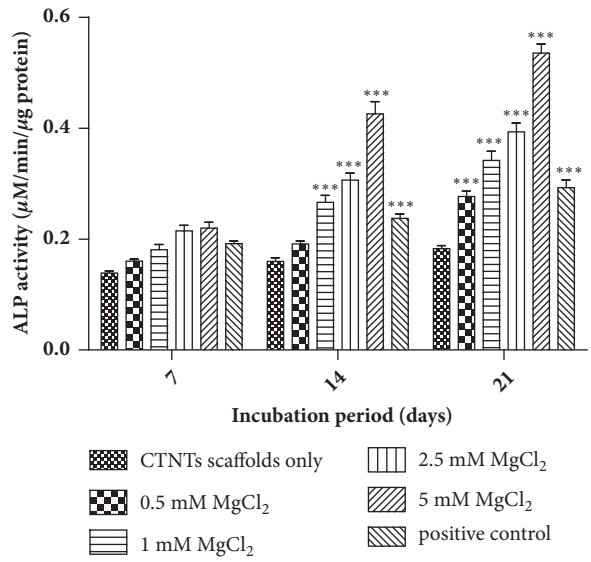

FIGURE 8: ALP activity of MG63 cells grown on CTNTs scaffolds only, CTNTs scaffolds functionalized with different amounts of Mg^{2+} ions and polystyrene well (positive control) on culture periods of 7, 14, and 21 days (∗ ∗ ∗p<0.001, n = 6).

control) throughout the assay as the poly-D-lysine coating on the commercial 24-well plates was deliberately fabricated to facilitate cell attachment and proliferation.

3.5. Early Differentiation Activity. Alkaline phosphatase (ALP) activity is an early differentiation marker for bone cells [31]. To verify the osteogenic property of CTNTs scaffolds, ALP activities of MG63 cells cultured on CTNTs scaffolds with and without Mg^{2+} ions for 7, 14, and 21 days were evaluated and the results are presented in Figure 8. There was no significant ALP activity difference between MG63 cells cultured on all types of scaffolds studied after 7 days of culture. The inhibitory effect of CTNTs scaffolds without Mg^{2+} ions on the proliferation of MG63 cells was followed by the impairment of early differentiation by showing low ALP activity. However, cells grown on scaffolds with Mg^{2+} ions were still in the proliferation stage after 7 days of culture as evidenced in Figure 7 which may not exhibit differentiation characteristics and this explained well their low ALP activity as observed (Figure 8).

On 14- and 21-day culture periods, MG63 cells grown on CTNTs scaffolds with Mg^{2+} ions showed significant upregulations of ALP activity in a concentration-dependent manner over those scaffolds without Mg^{2+} ions. The highest ALP activity was observed in MG63 cells grown on scaffolds functionalized with 5 mM $MgCl_2$ followed by 2.5 mM $MgCl_2$ after 21-day culture period. The ALP activity induced by CTNTs scaffolds functionalized with 5 mM $MgCl_2$ was approximately 3-fold higher than that of CTNTs scaffolds without Mg^{2+} ions. Further support has been evidenced by the cells cultured on polystyrene well without CTNTs scaffolds which did not show any apparent increment in ALP activity throughout the tested culture periods.

ALP is a vital element that is highly expressed in mineralized cells and hard tissue formation. Its overexpression activity was suggested to associate with the increased concentrations of mineralization promoter and inorganic phosphate and decreased concentration of the extracellular pyrophosphate, which is a mineral formation inhibitor [31]. The regulation of osteoblastic lineage cell differentiation involves complex transcription factors such as *RUNX2* and osterix (*OSX*) and signalling pathway [32]. The upregulated ALP activity of MG63 cells cultured on scaffolds with Mg^{2+} ions is possibly induced by $\alpha 5\beta 1$ integrin signalling in the presence of β-glycerol phosphate as soluble cues. The signalling seems to be amplified more with the increased amount of Mg^{2+} ions adsorbed on scaffolds, as the extracellular domain of integrin contains areas which bind to divalent cations. Our ALP finding is in fact conformed to the study conducted by Zreiqat et al. [16] in which the bioceramic substrata with Mg^{2+} ions showed an increased integrin expression.

Taken together, MG63 cells require a three-dimensional support like CTNTs scaffolds in order to initiate differentiation and the adsorbed Mg^{2+} ions onto CTNTs scaffolds have promoted the osteoblastic early differentiation more effectively. It may be attributed to the direct interaction between cell integrins and adsorbed Mg^{2+} ions [16, 30] which do not involve any conformation changes on scaffolds. This resulted in the activation of focal adhesion kinase (FAK) signal transduction pathway which is a prerequisite for the enhanced osteoblastic proliferation and early differentiation of MG63 cells cultured on scaffolds with Mg^{2+} ions. Yet, future investigations should involve more molecular studies to elucidate the effects of Mg^{2+}-functionalized CTNTs scaffolds on the mechanism of osteogenesis and expression of the later-stage osteodifferentiation and mineralization markers such as osteocalcin and osteopontin [1] before materializing the application of these scaffolds in bone regeneration.

4. Conclusions

The incorporation of TNTs into chitosan matrix at 16 wt% was attempted via direct blending, freezing, and freeze-drying. In functionalization, CTNTs scaffolds showed an exceptionally high adsorption affinity towards Mg^{2+} ions by uptaking 8.8 mg of Mg^{2+} ions per gram of scaffolds at 5 mM $MgCl_2$ concentration. Such isotherm fitted well with Langmuir isotherm which was indicative of monolayer adsorption. The chemisorption of Mg^{2+} ions onto CTNTs scaffolds was attributed to the nanocavities of TNTs. Different biological responses of MG63 cells were observed on CTNTs scaffolds with and without Mg^{2+} ions. The inherent low biocompatibility of CTNTs scaffolds was, however, overcome by the adsorbed Mg^{2+} ions. Scaffolds functionalized with more Mg^{2+} ions promoted better proliferation and early differentiation of MG63 cells by which 5 mM $MgCl_2$ concentration had accelerated these activities to the highest extent. This finding highlighted the significance of Mg^{2+} ions in influencing osteoblastic activities on CTNTs scaffolds in a concentration-dependent manner. In view of the said reinforced *in vitro* biocompatibility, CTNTs scaffolds functionalized with Mg^{2+} ions could be an alternative regenerative material for bone tissue engineering in the future.

Data Availability

No data were used to support this study.

Conflicts of Interest

The authors declare that there are no conflicts of interest regarding the publication of this paper.

Acknowledgments

This research project was financially supported by Ministry of Science, Technology and Innovation, Malaysia [03-02-12-SF0002]. Authors would like to extend gratitude to University of Nottingham Malaysia Campus for supporting the first author's PhD study and providing the facilities for this project.

References

[1] C. Y. Goh, S. S. Lim, K. Y. Tshai, A. W. Z. Z. El Azab, and H. S. Loh, "Fabrication and in vitro biocompatibility of sodium tripolyphosphate-crosslinked chitosan–hydroxyapatite scaffolds for bone regeneration," *Journal of Materials Science*, vol. 54, pp. 3403–3420, 2019.

[2] Y. Kuboki, H. Takita, D. Kobayashi et al., "BMP-induced osteogenesis on the surface of hydroxyapatite with geometrically feasible and nonfeasible structures: topology of osteogenesis," *Journal of Biomedical Materials Research Part B: Applied Biomaterials*, vol. 39, no. 2, pp. 190–199, 1998.

[3] P. Calvo, C. Remuñan-López, J. L. Vila-Jato, and M. J. Alonso, "Chitosan and chitosan/ethylene oxide-propylene oxide block copolymer nanoparticles as novel carriers for proteins and vaccines," *Pharmaceutical Research*, vol. 14, no. 10, pp. 1431–1436, 1997.

[4] Q. Hu, B. Li, M. Wang, and J. Shen, "Preparation and characterization of biodegradable chitosan/hydroxyapatite nanocomposite rods via in situ hybridization: a potential material as internal fixation of bone fracture," *Biomaterials*, vol. 25, no. 5, pp. 779–785, 2004.

[5] F. L. Mi, Y. C. Tan, H. F. Liang, and H. W. Sung, "In vivo biocompatibility and degradability of a novel injectable-chitosan-based implant," *Biomaterials*, vol. 23, no. 1, pp. 181–191, 2002.

[6] D. Raafat, K. von Bargen, and A. Haas, "Insights into the Mode of Action of Chitosan as an Antibacterial Compound," *Applied and Environmental Microbiology*, vol. 74, no. 12, pp. 3764–3773, 2008.

[7] M. Ishihara, K. Ono, Y. Saito et al., "Photocrosslinkable chitosan: An effective adhesive with surgical applications," *International Congress Series*, vol. 1223, no. C, pp. 251–257, 2001.

[8] E. Palin, H. Liu, and T. J. Webster, "Mimicking the nanofeatures of bone increases bone-forming cell adhesion and proliferation," *Nanotechnology*, vol. 16, no. 9, pp. 1828–1835, 2005.

[9] T. J. Webster, C. Ergun, R. H. Doremus, R. W. Siegel, and R. Bizios, "Enhanced functions of osteoblasts on nanophase ceramics," *Biomaterials*, vol. 21, no. 17, pp. 1803–1810, 2000.

[10] K. L. Elias, R. L. Price, and T. J. Webster, "Enhanced functions of osteoblasts on nanometer diameter carbon fibers," *Biomaterials*, vol. 23, no. 15, pp. 3279–3287, 2002.

[11] C. Yao, V. Perla, J. L. McKenzie, E. B. Slamovich, and T. J. Webster, "Anodized Ti and Ti_6Al_4V possessing nanometer surface features enhances osteoblast adhesion," *Journal of Biomedical Nanotechnology*, vol. 1, no. 1, pp. 68–73, 2005.

[12] S. S. Lim, C. Y. Chai, and H. S. Loh, "In vitro evaluation of osteoblast adhesion, proliferation and differentiation on chitosan-TiO_2 nanotubes scaffolds with Ca^{2+} ions," *Materials Science and Engineering C*, vol. 76, pp. 144–152, 2017.

[13] S. Kubota, K. Johkura, K. Asanuma et al., "Titanium oxide nanotubes for bone regeneration," *Journal of Materials Science: Materials in Medicine*, vol. 15, no. 9, pp. 1031–1035, 2004.

[14] W. W. Thein-Han and R. D. K. Misra, "Biomimetic chitosan-nanohydroxyapatite composite scaffolds for bone tissue engineering," *Acta Biomaterialia*, vol. 5, no. 4, pp. 1182–1197, 2009.

[15] K. Anselme, P. Davidson, A. M. Popa, M. Giazzon, M. Liley, and L. Ploux, "The interaction of cells and bacteria with surfaces structured at the nanometre scale," *Acta Biomaterialia*, vol. 6, no. 10, pp. 3824–3846, 2010.

[16] H. Zreiqat, C. R. Howlett, A. Zannettino et al., "Mechanisms of magnesium-stimulated adhesion of osteoblastic cells to commonly used orthopaedic implants," *Journal of Biomedical Materials Research Part B: Applied Biomaterials*, vol. 62, no. 2, pp. 175–184, 2002.

[17] Y. Yamasaki, Y. Yoshida, M. Okazaki et al., "Action of FGMgCO3Ap-collagen composite in promoting bone formation," *Biomaterials*, vol. 24, no. 27, pp. 4913–4920, 2003.

[18] M. Okazaki, "New type scaffold biomaterials with magnesium accelerating osteoblast adhesion and bone formation," *Journal of Oral Tissue Engineering*, vol. 1, no. 1, pp. 31–40, 2004.

[19] Q. Chen, W. Zhou, G. H. Du, and L. M. Peng, "Trititanate nanotubes Made via a Single Alkali Treatment," *Advanced Materials*, vol. 14, p. 1208, 2002.

[20] E. Morgado Jr, P. M. Jardim, B. A. Marinkovic et al., "Multistep structural transition of hydrogen trititanate nanotubes into

TiO2-B nanotubes: a comparison study between nanostructured and bulk materials," *Nanotechnology*, vol. 18, no. 49, Article ID 495710, 2007.

[21] Y. S. Ho and G. McKay, "The kinetics of sorption of divalent metal ions onto sphagnum moss peat," *Water Research*, vol. 34, no. 3, pp. 735–742, 2000.

[22] M. Hosseini, S. F. L. Mertens, M. Ghorbani, and M. R. Arshadi, "Asymmetrical Schiff bases as inhibitors of mild steel corrosion in sulphuric acid media," *Materials Chemistry and Physics*, vol. 78, no. 3, pp. 800–808, 2003.

[23] S. W. Lim, H. S. Loh, K. N. Ting, T. D. Bradshaw, and Z. N. Allaudin, "Reduction of MTT to Purple Formazan by Vitamin E Isomers in the Absence of Cells," *Tropical Life Sciences Research*, vol. 26, no. 1, pp. 111–120, 2015.

[24] J. R. Paletta, F. Mack, H. Schenderlein et al., "Incorporation of osteoblasts (MG63) into 3D nanofibre matrices by simultaneous electrospinning and spraying in bone tissue engineering," *European Cells & Materials*, vol. 21, p. 384, 2011.

[25] W.-Q. Yu, X.-Q. Jiang, F.-Q. Zhang, and L. Xu, "The effect of anatase TiO_2 nanotube layers on MC3T3-E1 preosteoblast adhesion, proliferation, and differentiation," *Journal of Biomedical Materials Research Part A*, vol. 94, no. 4, pp. 1012–1022, 2010.

[26] D. N. Furlong and G. D. Parfitt, "Electrokinetics of titanium dioxide," *Journal of Colloid and Interface Science*, vol. 65, no. 3, pp. 548–554, 1978.

[27] A. Hu, T. Lei, M. Li, C. Chang, H. Ling, and D. Mao, "Preparation of nanocrystals hydroxyapatite/TiO2 compound by hydrothermal treatment," *Applied Catalysis B*, vol. 63, no. 1-2, pp. 41–44, 2006.

[28] I. F. Amaral, M. Lamghari, S. R. Sousa, P. Sampaio, and M. A. Barbosa, "Rat bone marrow stromal cell osteogenic differentiation and fibronectin adsorption on chitosan membranes: the effect of the degree of acetylation," *Journal of Biomedical Materials Research Part A*, vol. 75, no. 2, pp. 387–397, 2005.

[29] M. Vandrovcova, J. Hanus, M. Drabik et al., "Effect of different surface nanoroughness of titanium dioxide films on the growth of human osteoblast-like MG63 cells," *Journal of Biomedical Materials Research Part A*, vol. 100, no. 4, pp. 1016–1032, 2012.

[30] A. P. Mould, S. K. Akiyama, and M. J. Humphries, "Regulation of Integrin $\alpha 5\beta 1$-Fibronectin Interactions by Divalent Cation-sevidence for distinct classes of binding sites for mn^{2+}, Mg^{2+}, AND Ca^{2+}," *Journal of Biological Chemistry*, vol. 270, p. 26270, 1995.

[31] E. E. Golub and K. Boesze-Battaglia, "The role of alkaline phosphatase in mineralization," *Current Opinion in Orthopaedics*, vol. 18, no. 5, pp. 444–448, 2007.

[32] F. Long, "Building strong bones: molecular regulation of the osteoblast lineage," *Nature Reviews Molecular Cell Biology*, vol. 13, no. 1, pp. 27–38, 2012.